Journal Title
XX(X):1–14
©The Author(s) 0000
Reprints and permission:
sagepub.co.uk/journalsPermissions.nav
DOI: 10.1177/ToBeAssigned
www.sagepub.com/
SAGE

Effect of the Exhaust Thermal Insulation on the Engine Efficiency and the Exhaust Temperature under Transient Conditions

Francisco J. Arnau[1], Jaime Martín[1], Pedro Piqueras[1], Ángel Auñón[1]

Abstract

As well as new advances in the after-treatment systems are required to achieve the new pollutant emission requirements, new designs of the exhaust line can be considered in order to increase the engine efficiency and the after-treatment effectiveness. In the present work, a one-dimensional gas dynamic model has been used to carry out a simulation study comparing several exhaust insulation solutions. This solutions include the insulation of the exhaust ports, the exhaust manifold, the internal surface of the turbine volute, the turbine external housing, as well as different combinations of these solutions. A transient analysis has been done in order to evaluate the increment in the exhaust gases temperature, fuel economy and pollutant emission levels over the WLTC (Worldwide harmonized Light vehicles Test Cycle) at three different temperature conditions. As a conclusion, a 12% increment in the turbine outlet gas enthalpy can be achieved by insulating both the exhausts ports and the exhaust manifold. Moreover, more than 30% less pollutant emissions are released to the environment with this setup.

Keywords

Exhaust insulation, turbine insulation, thermal management, light-duty diesel engine, aftertreatment thermal management, one-dimensional model, World Harmonized Light-duty Vehicle Test Procedure, light-off temperature, diesel engine emissions

Introduction

During the last years, the emissions legislation in the major automotive regions have established more restrictive limits of the air pollutants released into the atmosphere in order to reduce the environmental impact of the transportation activities[1]. For this purpose, to minimize fuel consumption and emissions has become one of the major goals of engine developers and manufacturers. Specially in diesel engines, a great challenge is the cold start and heating phase, since heating techniques are a compromise between a fast heat-up of the after-treatment system and a low penalty in fuel consumption.

Several studies have been performed addressing the topic of the exhaust thermal management. Arnau et al.[2] studied the potential that variable valve timing and a second exhaust valve event have in increasing the exhaust gas temperature. Their results showed that an increment of 50°C in the exhaust temperature, associated with a fuel penalty of 5%, can be obtained by advancing the exhaust and delaying the intake valve events. Luján et al.[3] studied the possibility of placing the after-treatment system, a DOC coupled to a DPF, before the turbine in order to benefit the pollutants oxidation and the DPF passive regeneration.

A major breakthrough in diesel engine technology has been achieved by the pioneering work done by Kamo and Bryzik, since the end of the 1970s, as the first persons in introducing TBC system for engines[4,5]. Kamo and Bryzik used thermally insulating materials such as silicon nitride for insulating different surfaces of the combustion chamber. The application of thermal barrier coatings (TBC) in thermal engines has been widely explored as a way to reduce the heat rejected in the combustion chamber[6–11] in order to improve engine efficiency and reduce NO_x emissions.

Some authors have studied the application of thermal barrier coatings in the insulation of exhaust manifolds. EkstrÖm et al.[12] analyzed several types of barrier coatings to insulate the internal walls of a diesel engine exhaust manifold for improving its fatigue life. Their results showed that it is possible to reduce the temperature in the metal up to 50°C by applying a 3mm thick layer of a TBC with a thermal conductivity of 1.5 W/m K, like, for instance, YSZ (yttria-stabilized zirconia). Working towards this direction, Thibblin et al.[13] experimentally studied the thermal cyclic life of different TBCs in a heavy-duty diesel engine exhaust manifold.

Kishi et al.[14] studied the thermal insulation of a gasoline exhaust manifold and its impact on the exhaust gas temperature and hydrocarbon emissions. Their results, in combination with an engine with variable valve timing, shown an increment in the exhaust gas temperature as well as an 8% increment in HC conversion efficiency.

[1]CMT - Motores Térmicos, Universitat Politècnica de València, ES

Corresponding author:
Francisco José Arnau Martínez, CMT - Motores Térmicos, Universitat Politècnica de València,
Camino de Vera s/n, Valencia 46022, Spain
Email: farnau@mot.upv.es

Zidat and Parmentier[15] studied the internal and external heat transfer in exhaust manifolds to minimize the catalyst light-off time. They concluded that the internal heat transfer is most dominant mode of heat loss from the exhaust manifold. Reducing the internal heat transfer will significantly increase the catalyst temperature. Moreover, external heat insulation becomes more and more important as the exhaust manifold gets warmer.

A more recent study carried out by Serrano et al.[16]. They experimentally tested the thermal insulation of the combustion chamber and the exhaust manifold in a six cylinder heavy-duty engine. According to their results, a 1% specific fuel consumption reduction was obtained by insulating the exhaust manifold. Furthermore, a slight improvement in both NO_x-Soot and NO_x-BSFC was achieved, compared to other solutions concerning the insulation of the pistons and the cylinder head.

Considering how the insulation of the exhaust ports and the turbine affects the temperature upstream the after-treatment systems, Luján et al.[17] performed a numerical study of the potential of thermal insulation of these elements in steady-state operating conditions.

In the work presented in this paper, a simulation study is presented comparing different exhaust thermal insulation solutions in dynamic conditions of speed and load, taking the WLTC class 3 test cycle as the reference. These solutions consider the division of the exhaust system in 3 parts: ports, manifold and turbine. The different solutions represent the insulation of these elements and some combinations of them. With the aim of understanding the influence of each element in the catalyst inlet temperature, each solution assumes an adiabatic insulation of the elements involved in it. It means, for instance, that the insulation of the exhausts ports assumes no heat transfer between the hot gases and the surface of these ports. The results obtained are discussed in terms of fuel economy, exhaust gas temperature increase, HC and CO conversion efficiencies and HC and CO pollutant emissions reduction.

Experimental setup

This work has been performed based on a calibrated and validated HSDI Diesel engine model. This engine is a 1.6L four-stroke engine compliant with Euro 5 emissions regulations whose specifications can be found in Table 1. From the point of view of thermal management, the low pressure EGR is cooled by a gas-coolant heat exchanger, and another gas-coolant heat exchanger cools the intake air to the cylinders. In order to reduce the warm-up time, the engine includes an electrovalve that blocks coolant flow through the engine block during engine warming. The turbocharger system consists of a radial compressor and a variable geometry turbine (VGT). This turbocharger is not refrigerated by water, but all the heat coming from the turbine and mechanical losses are dissipated by the lubricating oil. The location of the turbocharger within the lubrication circuit is shown in Figure 5. Finally, the after-treatment system consists of a close-coupled DOC and DPF brick.

The test cell consists of a climate dynamic room, which allows performing cold start tests (down to -15°C). The test cell is fully equipped to measure operation mean variables and in-cylinder pressures in the four cylinders. It also includes a Horiba MEXA-One exhaust gas analyzer along with an AVL439 Opacimeter. Table 2 summarizes the relevant instruments used for this study. Data was acquired at a frequency of 10Hz with a test automation system.

Table 1. Engine specifications.

Type	EURO 5 HSDI Diesel engine
Displacement	1598 cm^3
Stroke	79.5 mm
Bore	80 mm
Compression ratio	14.5:1
Number of valves	4 per cylinder (2 int., 2 exh.)
Number of cylinders	4 in line
Air management	VGT, LP-EGR, HP-EGR
EAT System	Closed-coupled DOC + DPF
Max. power @ speed	96 kW @ 4000 rpm
Max. torque @ speed	320 Nm @ 1750 rpm

Table 2. Test cell instrumentation.

Variable	Instrument	Range	Accuracy
Crank angle	Encoder	0-360°	±0.02°
Torque	Dynamometer	0-400 Nm	±0.5 Nm
Gas/wall temperature	k-type thermocouple	70-1520 K	±2 K
Air mass flow	Sensyflow DN80	0-1700 hg/h	±2 %
Coolant flow	Krohne 400 Optiflux	4.5-90 L/min	±0.5 %
Oil pressure	Piezoresistive transducer	0-10 bar	±25 mbar
In-cylinder pressure	AVL GH13P	0-200 bar	Linearity 0.3 %

The engine layout is depicted in Figure 1, where the main components of the engine and the temperature and pressure measurement points are indicated. These points correspond to the intake and exhaust manifolds, and the inbound and outbound ducts of both compressor and turbine. The pollutant emissions points were measured upstream the after-treatment system, in order to calibrate the emissions sub-model. For the validation of the DOC and DPF sub-models, exhaust were measured upstream and downstream the after-treatment system, as it is explained by Payri et al.[18]. The four different colored regions in Figure 1, represent the exhaust ports, exhaust manifold and turbine internal layer and turbine external casing. These zones have been insulated in the engine model and simulated representing 8 different cases: the thermal insulation of these 4 exhaust parts and 4 combinations of them. The colors indicated here are the same used later for graphs in the results section.

Model setup and validation

This section addresses the engine model used throughout this work. First, the virtual engine model software is introduced, briefly presenting the different sub-models that make up the engine model. Finally, the validation process at transient operating conditions is discussed.

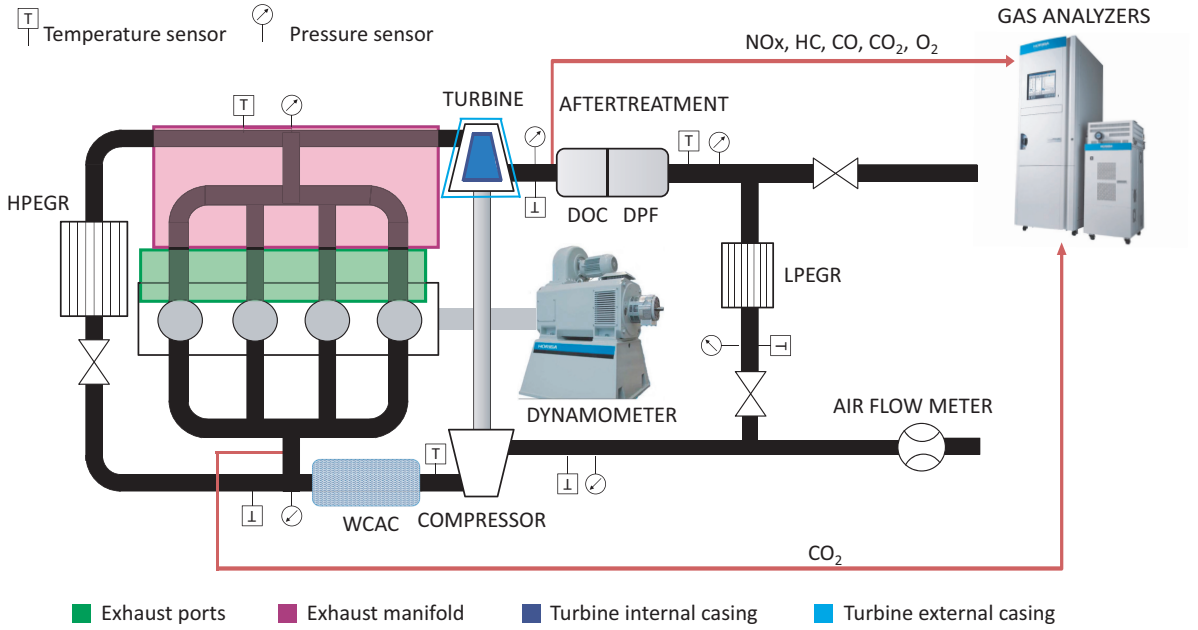

Figure 1. Engine layout with the pressure, temperature and exhaust gases measurement points.

Virtual engine model (VEMOD)

The gas dynamics software VEMOD [19] has been used for this study. In VEMOD the air management is computed by means of a 1D gas dynamics model which performs the calculations of the flow properties along the intake and exhaust systems as well as the high and low pressure EGR paths. Thus, specific sub-models are considered for the boosting system [20,21], air-charge and EGR coolers, throttle valves, heat transfer including gas-to-wall heat exchange and wall temperature prediction, after-treatment sub-models (DOC and DPF), a 0D turbocharger model and a hydraulic circuit model. The gas dynamics model is coupled to a cylinder model that predicts the in-cylinder conditions based on the combustion process. Detailed heat transfer model is used to obtain the heat rejection to the chamber walls while mechanical losses model allows obtaining the brake power. An emission sub-model is coupled to the combustion process to predict raw NOx, CO, HC, and soot emissions as a function of the engine operating conditions. Figure 2 represents the air path systems present in the virtual engine model. Different systems have been remarked in the scheme, such as the intake and exhaust manifolds, the turbocharger and the high and low pressure paths, as well as the positions of the sensors that send data to the virtual ECU model.

The turbocharger is based on 0D compressor and turbine sub-models. They use the data provided by the supplier maps for both turbine and compressor to compute the flow and the turbomachines efficiencies at any operating point within the maps. Besides, the model is able to extrapolate outside these maps so it is possible to simulate off-design conditions [22]. The turbocharger sub-model also simulates the heat transfer and the mechanical losses by means of a lumped heat transfer model, whose diagram is shown in Figure 3, hence improving the prediction of the turbine outlet temperature prediction and the heat fluxes involved in the turbocharger. As depicted from the diagram, a fraction of the exhaust gases energy is not converted into work in the turbine and is transferred as heat to the ambient, the lubricating oil and other metal parts of the turbocharger. Further details of this heat transfer sub-model and an analysis of the effect of the turbocharger heat and mechanical losses are explained in [23,24].

The combustion and emissions sub-model consists of a 1D model able to predict the combustion profile and the main pollutant emissions with an acceptable accuracy. For the sake of completeness, the IMEP relative error is about 3% and the NO_x emissions error is about 8% throughout the WLTC [19]. The combustion model is composed of three main sub-models: ignition delay, premix combustion and diffusion combustion models; along with a 1D model describing the mixing process. A detailed description of the model can be found in [25,26].

The hydraulic circuits sub-model, allows calculating mass flow and temperatures of oil and coolant at different engine components like the engine block galleries, the EGR coolers, the turbocharger and the oil and coolant pumps. Hydraulic circuit elements like thermostats, operable valves, pumps and heat exchangers have been modeled and simulated. The coolant circuit (Figure 4) and the oil circuit (Figure 5) are based on a thermo-hydraulic network composed of branches, meshes and nodes. By applying the continuity and conservation laws, the mass flows and head losses of the hydraulic networks are calculated. In order to calculate the temperature distribution, the branches (a pipe between two nodes) are divided into several fluid volumes or parcels. Simultaneously, the heat exchanger sub-model updates the temperatures. Further details regarding the hydraulics sub-models are collected in [27].

Figure 6 shows the flow-chart of the virtual engine model. The blue boxes represent the thermo and fluid dynamics sub-models described above, while the red boxes represent the different control sub-models, which have been developed in Matlab/Simulink. They operate the engine model by actuating over the different actuators defined in the engine

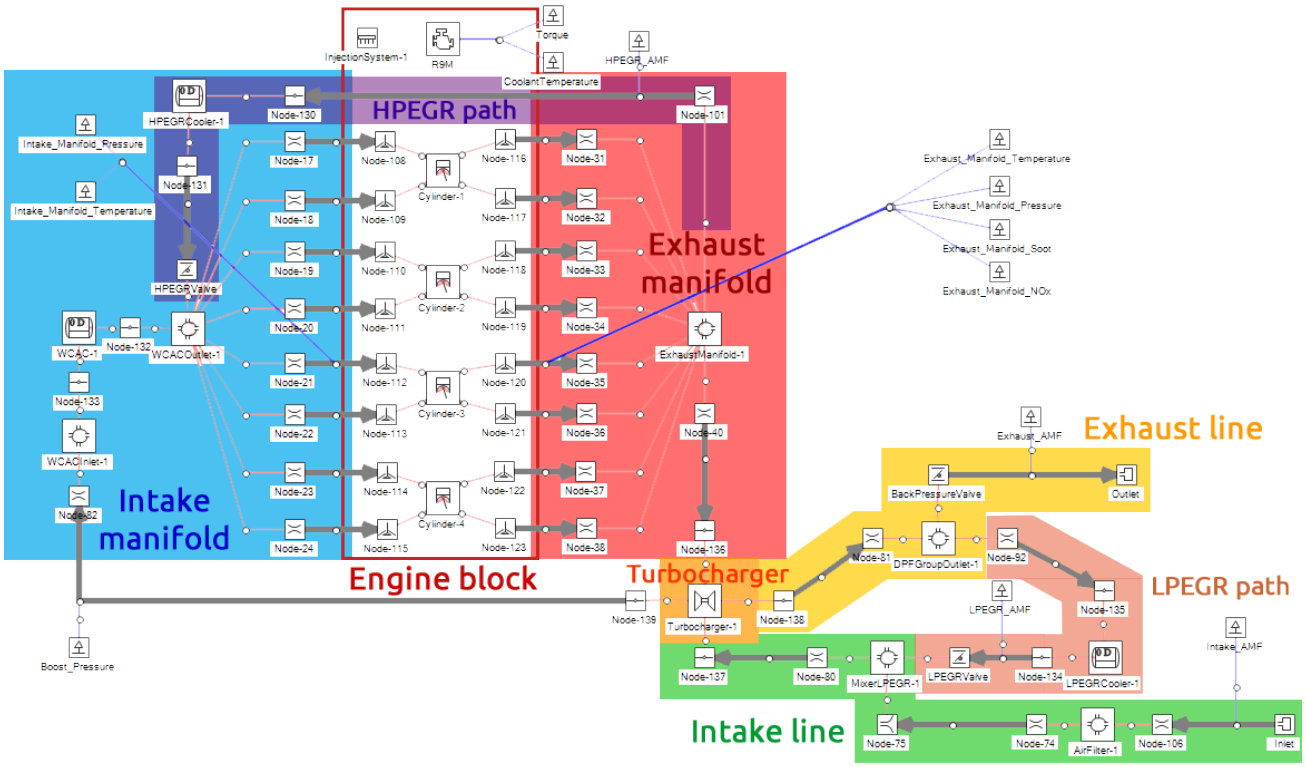

Figure 2. Model scheme of the 1D engine model in VEMOD software.

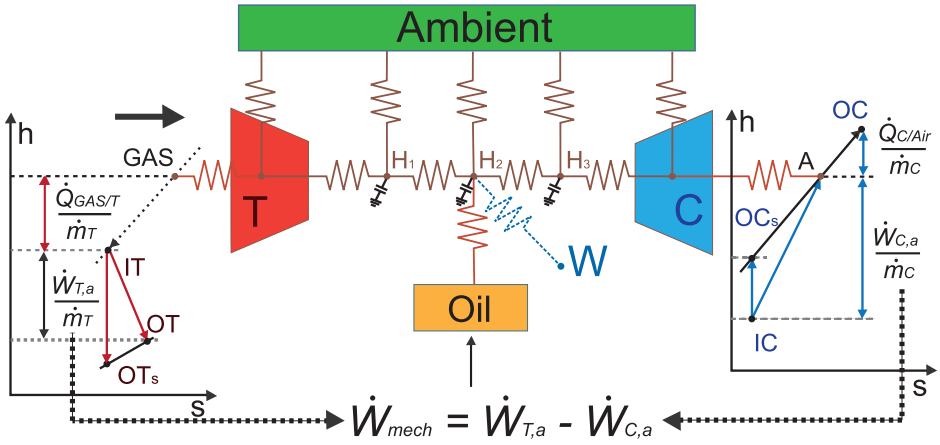

Figure 3. Scheme of the turbocharger lumped heat transfer model.

model. The driver and vehicle model can be detached from the control sub-model if just the engine speed and torque setpoints are provided.

Throughout this study, all the simulations were performed keeping the torque of the baseline case, which is the one with original exhaust system. In order to achieve this objective, a control system included in VEMOD has been used. The control model emulates the ECU to control the injection by modifying the injection pressure, the fuel mass split and the start of injection depending on engine speed and total fueling rate. The model also controls the air loop by means of the VGT rack position (whose control is based on the intake pressure setpoint, depending on engine speed and total fueling rate), and LP-EGR, HP-EGR and back pressure valves, which control is based on the air mass flow setpoint. For any specific engine speed and torque, the required fuel mass is obtained from a calibration map. Once the engine speed and fuel mass are known, the injection pulses timings and masses, intake manifold pressure setpoint, injection pressure and air mass flow setpoints are obtained from their respective maps. These maps were created on the basis of a series of 23 steady-state points spread throughout the entire engine map and using the baseline valve-train configuration.

The calibration process and the results in terms of burn rate, in-cylinder pressure, mechanical losses, pollutant emissions, as well as detailed information about the different sub-models are described in [19].

Model validation at transient operating conditions

In Figure 7 several variables are represented comparing experimental measurements versus model results. Figure 7a shows engine brake torque with a coefficient of

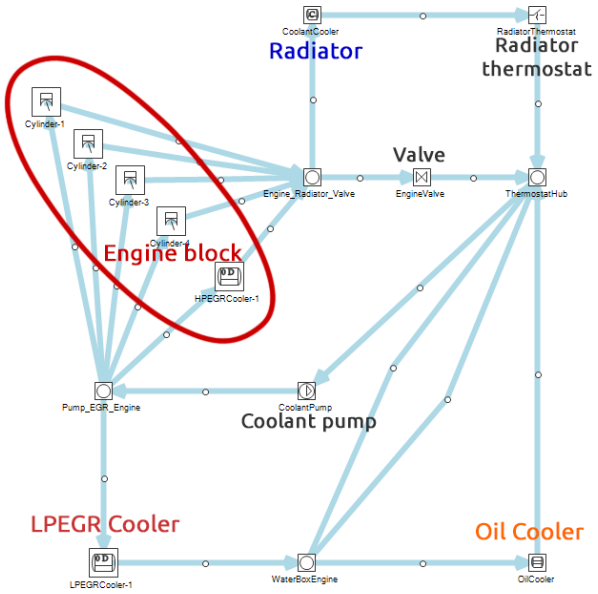

Figure 4. Model scheme of the 1D coolant circuit in VEMOD software.

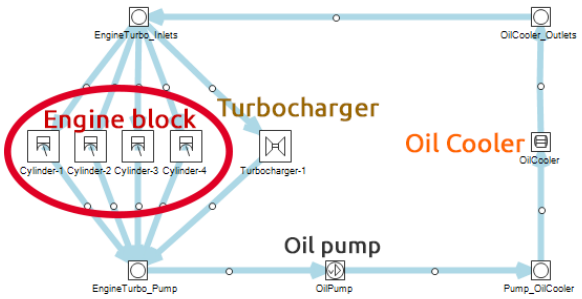

Figure 5. Model scheme of the 1D lubrication circuit in VEMOD software.

determination (R^2) of 0.938. This comparison has been done by imposing the experiment fuel mass at each time step of the simulation. The air mass flow target is controlled by the ECU sub-model actuating over the VGT position and the EGR valves. The resulting simulated torque is accurate all along the WLTC.

Figure 7b shows the turbine outlet temperature, which coincides with the gas temperature at DOC inlet. It is interesting to analyze how different insulation configurations affect EAT inlet temperature, particularly during the warm-up time. The faster the light-off temperature (defined as the temperature at which conversion efficiency reaches 50%) on the catalyst is reached, the faster the efficient oxidation of CO and HC, and the oxidation of NO to NO_2, is achieved. This light-off temperature is considered to be around 200°C according to an averaged space velocity of 57700 h^{-1} during the WLTC[28,29]. The decrease in DOC-out NO_2 may have a negative effect on downstream NO_x abatement, specially at temperatures below 250°C, such as those at engine start up[30]. Moreover, DOC conversion efficiency increases as the temperature grows[18,31], so an increment in DOC inlet temperature can be profitable. The model is able to follow well the turbine outlet temperature trend, specially during the

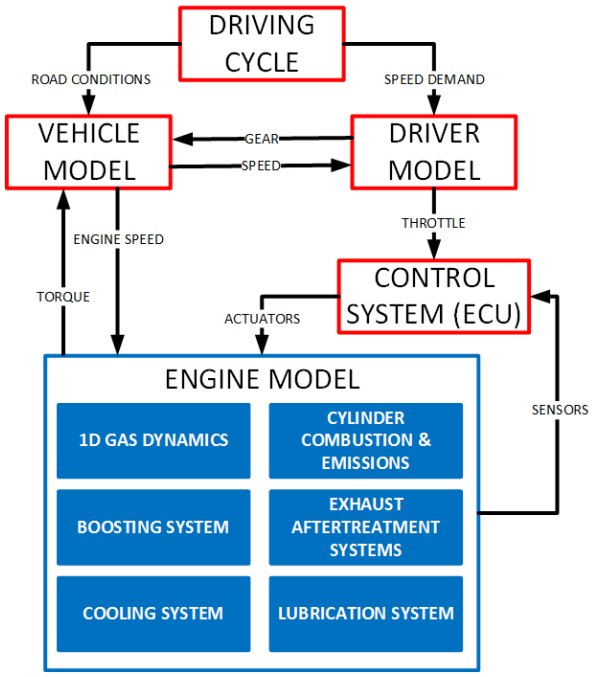

Figure 6. Flow-chart of VEMOD modules.

medium and high speed part of the WLTC, where the percent error is below 10%.

Coolant temperature at cylinders outlet is shown in Figure 7c. In this case, a medium total error of −2°C along the whole cycle was obtained. Since the coolant temperature has a slight effect on the volumetric efficiency and consumption, and some effect on NO_x formation[32,33], it is interesting to achieve a good prediction. According to the authors, an increase in the coolant temperature leads to an increment of the cylinder wall temperature, which increases the air temperature during the intake stroke, and results in a decrease of the air density. This cylinder wall temperature increment also has some impact on the NO_x formation, specially at low load[33].

Figure 7d and Figure 7e show NO_x and CO accumulated emissions at engine outlet, right upstream the after-treatment system. In both cases, the overall formation is well reproduced along the WLTC. However, CO formation prediction is underestimated, specially at high engine speed. On the contrary, NO_x formation is overestimated. This overestimation is shown very clearly during the high speed stretch of the WLTC, where NO_x formation increases.

Regarding hydrocarbon emissions, Figure 7f shows a good prediction of total HC at engine outlet. It can be seen a little overestimation at the beginning of the cycle. Contrarily, the model underestimates the THC emissions formation at high speed and high load.

The validation at a room temperature of −7°C is presented in Figure 8. The model is able to reproduce the experimental torque (Figure 8a) with a coefficient of determination of 0.936. The torque is well predicted all along the cycle, but with an small error for the accelerations in the first 100 seconds due to small uncertainties of the sub-models at cold conditions.

The turbine outlet temperature prediction, shown in Figure 8b, tends to be slightly higher than the measured one,

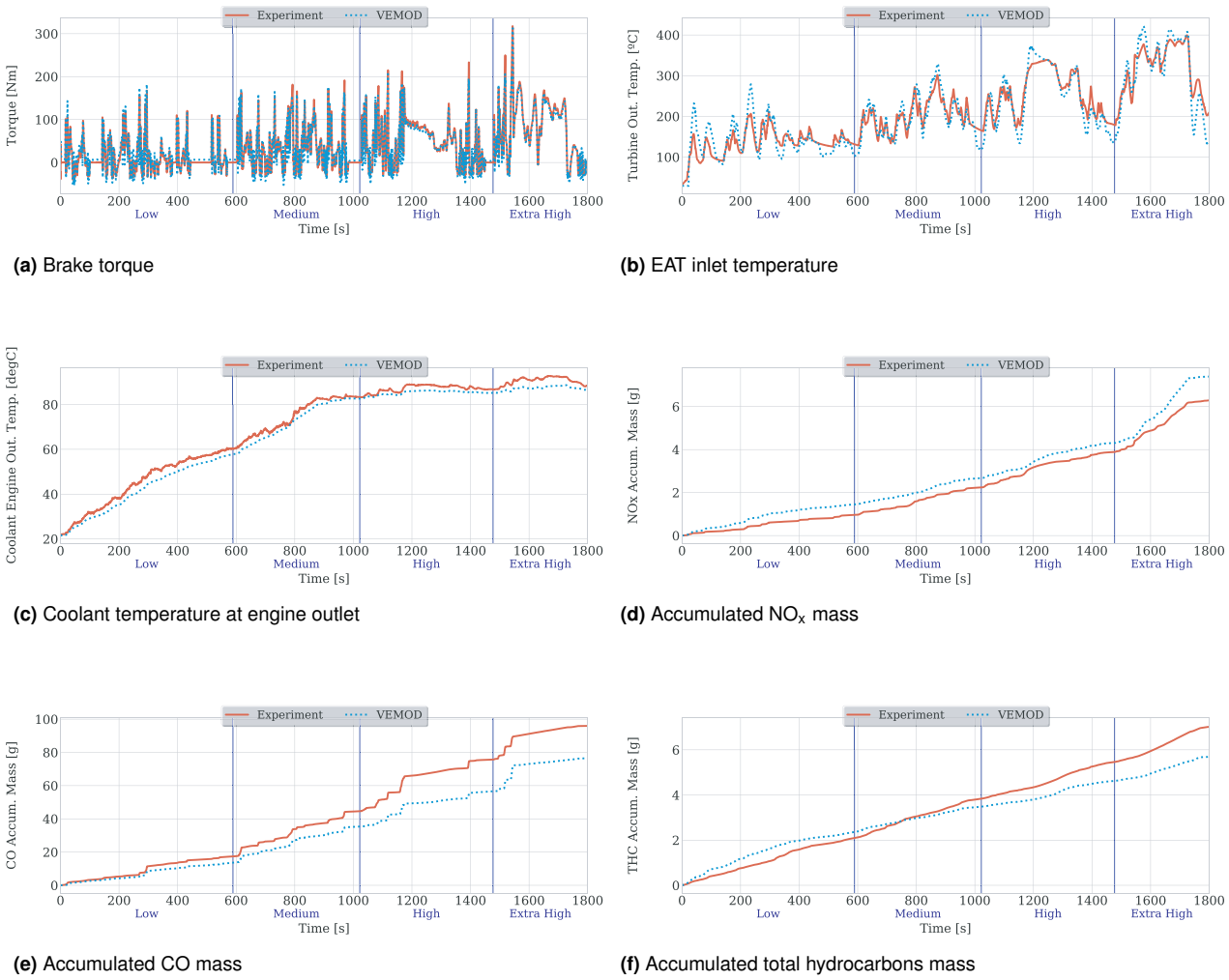

(a) Brake torque

(b) EAT inlet temperature

(c) Coolant temperature at engine outlet

(d) Accumulated NO_x mass

(e) Accumulated CO mass

(f) Accumulated total hydrocarbons mass

Figure 7. WLTC model validation, engine start at 20°C room temperature.

compared to the the prediction at 20°C. These temperature difference is evident during the first 100 seconds and at the highest temperature values in the high and extra high speed periods of the cycle. However, all the temperature variations are followed and the percent error for the medium and high speed parts remains around 10%.

Concerning the warm-up of the engine coolant at a test bench temperature of −7°C (Figure 8c), it is faster than the warm-up prediction at a room temperature of 20°C. This is caused by the heat repartition in the engine block. At these cold conditions, the model is underestimating the heat transferred from the block to the ambient and, consequently, overestimating the heat amount dissipated by the coolant as it flows through the engine block.

Regarding pollutant emissions at engine outlet, the NO_x formation prediction in Figure 8d is well followed. In this case at −7°C, the final accumulated value is lower than the one of the experiment, but the main trend along the cycle is that the model overestimates the NO_x formation. The CO formation prediction at *Cold* conditions is not so good as the previous results. The model clearly underestimates the CO production, as it can be seen in Figure 8e.

With respect to total hydrocarbons formation, Figure 8f shows that the model follows the experimental trend, however the total HC formation is underestimated for the whole transient cycle.

The CO and HC emissions formation are predicted by using a neural network approach. This neural network has been trained using data from steady-state operating points. It can be observed that, due to this training process, the model does not properly reproduce the emissions during the fast accelerations. Hence, the final accumulated values are lower than the real ones, specially at −7°C. In advance in this work, all the emissions comparisons are done in relative terms: comparing the different insulation cases with respect to the baseline (not insulated) case. Thereby, some trends can be identified and compared between the different stages of the WLTC standard cycle.

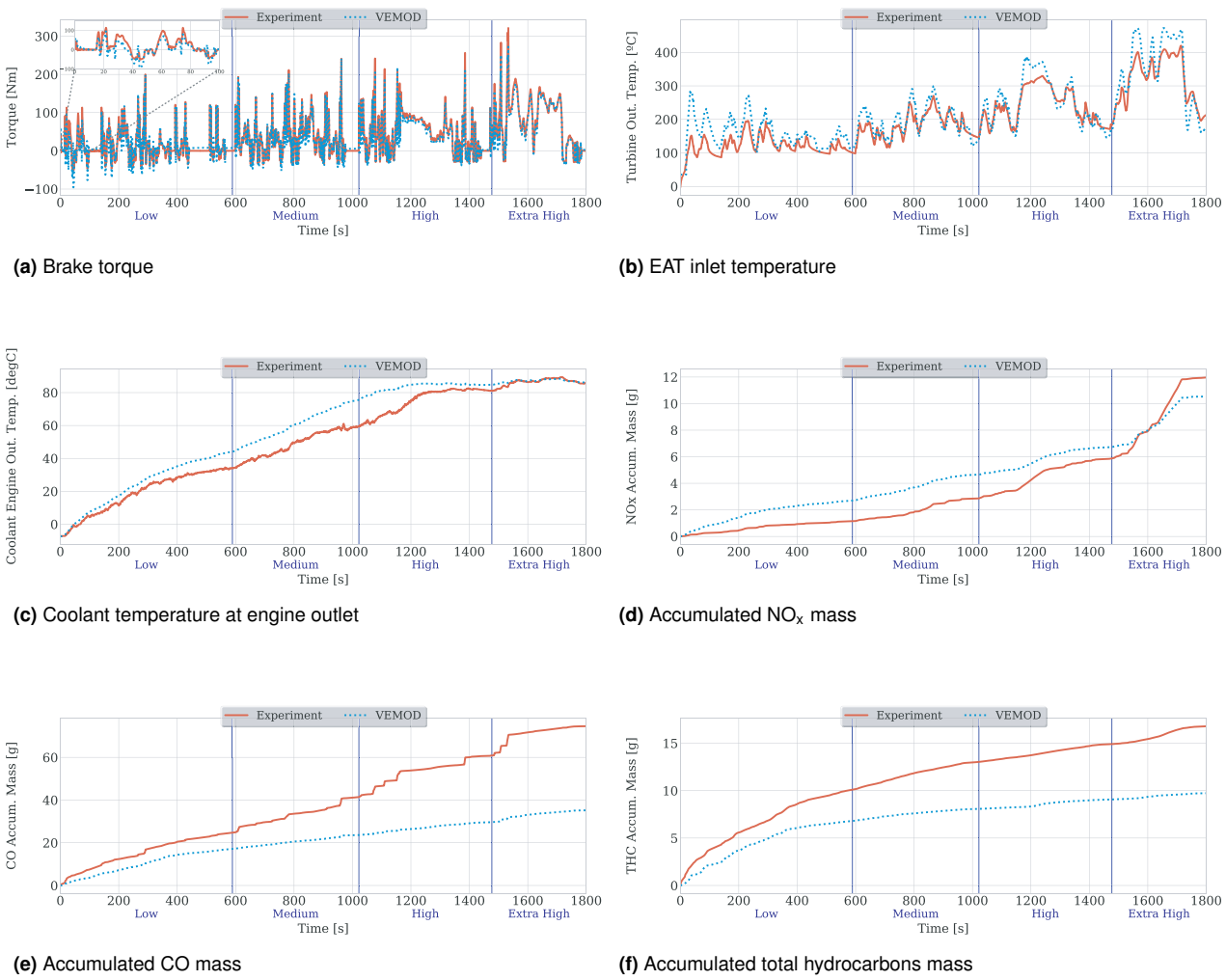

Figure 8. WLTC model validation, engine start at -7°C room temperature.

Methodology

This work is centered on how the exhaust temperature can be increased by insulating the different parts of the engine's exhaust line. These elements, or parts of the exhaust line, are the engine exhaust ports, the exhaust manifold and the turbine. In this study, all these elements have been fully insulated, making them adiabatic, in order to have an idea of the maximum increment in the exhaust temperature. According to this, nine different configurations have been simulated (four insulating only one of these elements and five as a combination of them). Table 3 summarizes the adiabatic elements for each configuration. Thus, the *Baseline* configuration does not consider any additional insulation, it represents the original engine model presented before. The *EP* configuration considers no heat transfer from the hot gases to the eight exhaust ports walls. In the *EM* case, there is no heat transfer between the exhaust gases and the exhaust manifold walls, including the volume between the exhaust ports and the turbine inlet section. The *TI* configuration considers no heat transfer between the exhaust gases and the turbine volute. The rest of configurations are a combinations of these four adiabatic cases. A special mention must be made for *Full Exhaust* case, which is the sum of the previous cases plus a completely insulated turbine housing; hence there is no convection between the metal and the ambient.

The main reason why there is not any configuration just insulating the external layer of the turbine housing, nor a combination with other configuration, is because it has no significant impact in the temperature at turbine outlet. The explanation for these poor performance of the external turbine insulation is due to the alternative path for the heat to be transferred along the turbocharger. Although there is no convection between the metal and the environment, the heat is driven axially through the metal and removed partially by the lubrication oil. This can be observed in Figure 9, where there is a great difference in the accumulated heat from the turbocharger to the ambient between cases *Baseline* and *TE* (turbine external insulation); whilst there is no such difference when it comes to the accumulated heat to oil. The same occurs if another configuration is considered and the same one plus the turbine external insulation (*EM* and *EM* + *TE*). Regarding the decline that can be seen in

Table 3. Simulation cases.

Cases	Heat transfer			
	Exhaust ports	Exhaust manifold	Turbine internal casing	Turbine external casing
Baseline	✓	✓	✓	✓
EP	O	✓	✓	✓
EM	✓	O	✓	✓
EP + EM	O	O	✓	✓
TI	✓	✓	O	✓
EP + TI	✓	✓	O	✓
EM + TI	✓	O	O	✓
EP + EM + TI	O	O	O	✓
Full Exhaust	O	O	O	O

✓: heat transfer unchanged, O: adiabatic

the accumulated heat to oil graphs (Figure 9), it happens because, at the end of the cycle, the temperature of the metal nodes in the turbocharger heat transfer model are greater than the temperature in the oil. This means that the heat flux goes from the metal to the oil, considered as negative; contrarily to what happens for more than half of the cycle, where the oil is hotter than the metal.

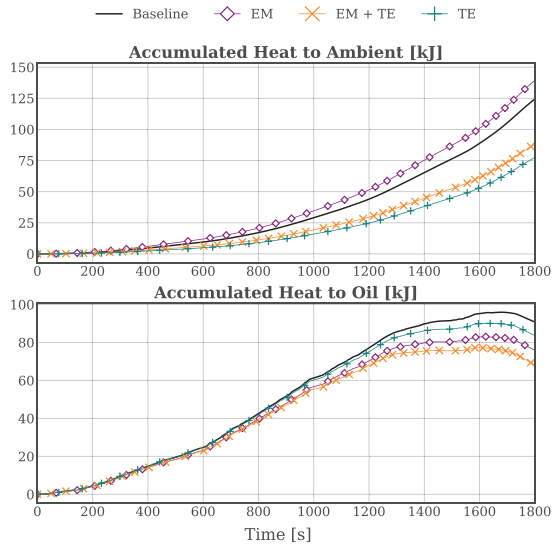

Figure 9. Accumulated turbocharger heat to ambient and heat to oil throughout the WLTC at ambient temperature.

In order to perform this study, the resulting torque from the *Baseline* simulation was imposed as the torque target for all the different insulation combinations. The ECU control model basically takes control on the fuel mass injected and the required air mass flow to reach the torque ant any operating point, based on the engine calibration that contains several maps for boost pressure, air mass flow and fuel injected. In this way, it is possible to quantify differences on fuel consumption, pumping losses, exhaust temperature and other key outputs when compared to the baseline configuration.

An analysis in transient conditions of engine speed and load has been carried out considering the Worldwide harmonized Light vehicles Test Cycle (WLTC) in three different temperature conditions. Table 4 lists these different conditions. Thus *Warm* refers to the WLTC at the room temperature of 20°C and an engine temperature near 80°C. The *Ambient* conditions refer to the WLTC at the room temperature of 20°C, but with the engine starting from cold. Finally, the *Cold* conditions refer to an engine cold start while keeping the room temperature at −7°C.

Results and discussion

The main goal for insulating the exhaust gases path is to achieve greater temperatures in order to increase the efficiency of the after-treatment devices and/or recover part of the available energy of the hot gases. The accumulated gas enthalpy downstream the turbine is presented in Figure 10 as the absolute difference with respect to baseline case. It can be observed that all the configurations achieve some increment in the exhaust enthalpy compared to the *Baseline* case in the three temperature conditions. As it was expected, the lowest increment is obtained by the *TI* configuration because it has less scope than any other for insulating since there are heat losses upstream the turbine. On the contrary, the *Full Exhaust* configuration performs best, achieving an increment of 3350 kJ (12.1%), 2920 kJ (12.0%) and 3365 kJ (14.5%) respect to the *Baseline* case at *Warm*, *Ambient* and *Cold*, respectively. In terms of temperature, it implies an increment between 50°C, at partial loads, to 100°C at full load. The results obtained by *EM* are better than *EP* configuration during the low speed stage of the WLTC; since, the exhaust manifold volume is higher than the one of the exhaust ports and the heat losses are greater during the heating process of the manifold. However, by the high speed part of the WLTC, when the exhaust ports are insulted, the advantage in heat retention are greater since the heat transfer in the exhaust manifold is lower than during the heating phase and the high load transients of this zone of the cycle contribute significantly to increase the exhaust enthalpy.

The rest of configurations achieve exhaust temperatures in between of these two alternatives. The configurations that are a combination of two perform right below the *Full Exhaust*. Comparing just the *EM* and *EP* alternatives, show that insulating the exhaust ports makes more sense in terms of heat recovery because the temperature of the gases is higher at this point. Consequently, *EP* achieves an increment in enthalpy around 1% higher than *EM*, going up to 2% in *Cold* conditions; since more energy is lost in these conditions where the thermal gradient between hot gases and the environment is higher and the metal parts are getting warmer throughout the transient.

Figure 11 shows the coolant temperature at engine outlet for each temperature condition (*Warm*, *Ambient* and *Cold*). In all the three conditions, the configurations in which the exhaust ports are insulated (*EP, EP + EM, EP + TI, EP + EM + TI,* and *Full Exhaust*) lead to a lower coolant temperature. This phenomenon is more evident during the warm-up period (*Ambient* and *Cold*), concluding with differences between 3

Table 4. Simulation transient conditions.

Name	Cycle	Engine temp.	Test cell temp.
Warm	WLTC	already warm ($\approx 80°C$)	$20°C$
Ambient	WLTC	cold start ($\approx 20°C$)	$20°C$
Cold	WLTC	cold start ($\approx -7°C$)	$-7°C$

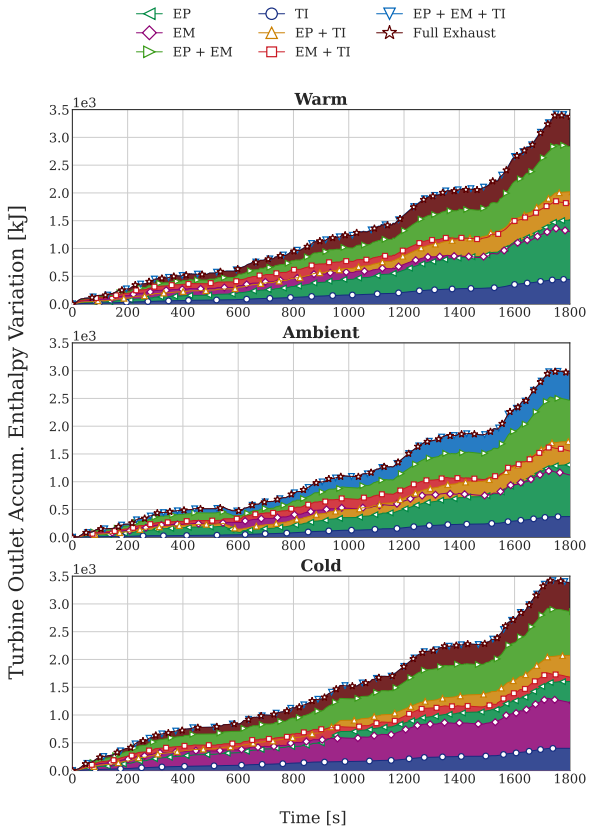

Figure 10. WLTC accumulated gas enthalpy at turbine outlet, difference respect to the baseline case.

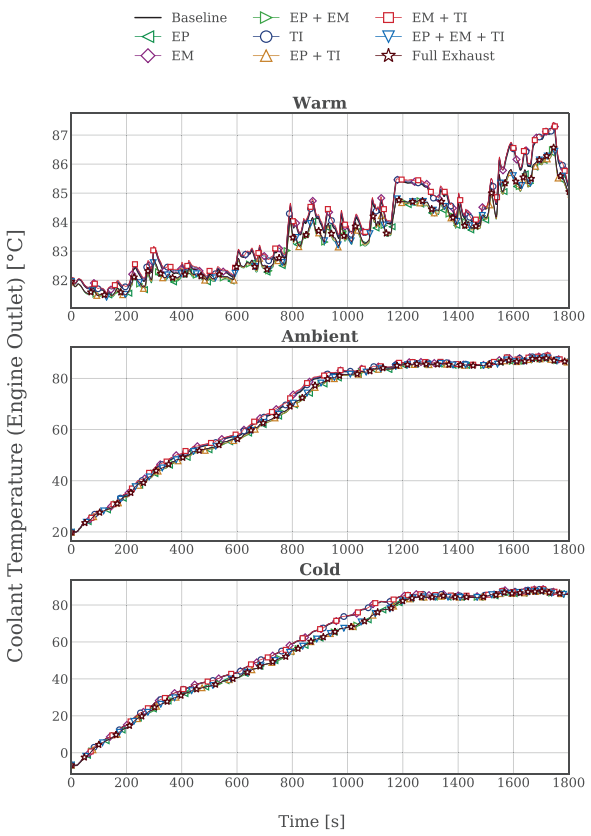

Figure 11. Coolant temperature at engine outlet throughout the WLTC transient cycle.

to 10 Celsius degrees respect to the *Baseline* case. When the exhaust ports are not completely insulated, a considerable amount of the heat is collected by the coolant circulating inside the cylinder head; thus explaining the temperature difference in these configurations.

The coolant temperature plays an important role in this engine when enabling the EGR system. In this particular EURO 5 engine, the activation of the two EGR routes depends on the intake temperature and the coolant temperature. According to this behavior, variations of the coolant temperature affects the activation of the EGR, leading to a direct effect on exhaust pollutant emissions. In the cases where the exhaust ports are insulated, the LP-EGR/HP-EGR activation is delayed, as it can be seen in Figure 12. At *Ambient* conditions, the delay in the LP-EGR activation is about 51 seconds for the *EP* case and 54 seconds for the *EP + TI* one. At *Cold* conditions there is no difference among these alternative and the delay in the HP-EGR activation is about 67 seconds.

Regarding pollutant emissions downstream the after-treatment, Figure 13 show the accumulated CO emitted mass variation (respect to the Baseline case) throughout the entire

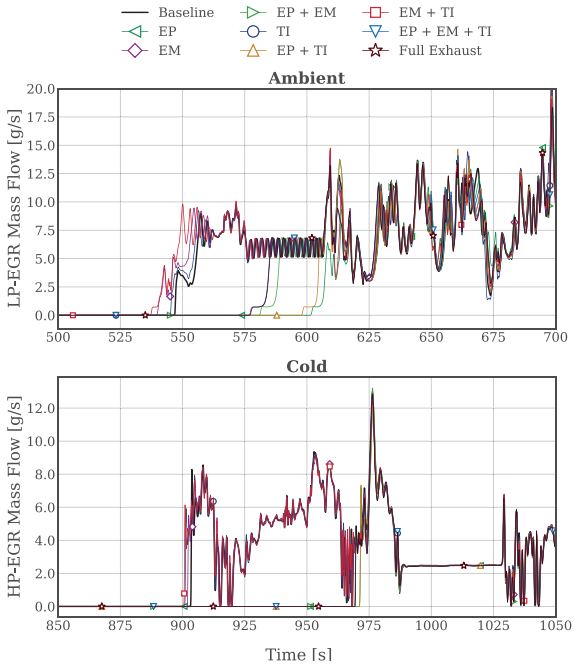

Figure 12. LP-EGR and HP-EGR activation at ambient and cold conditions, respectively.

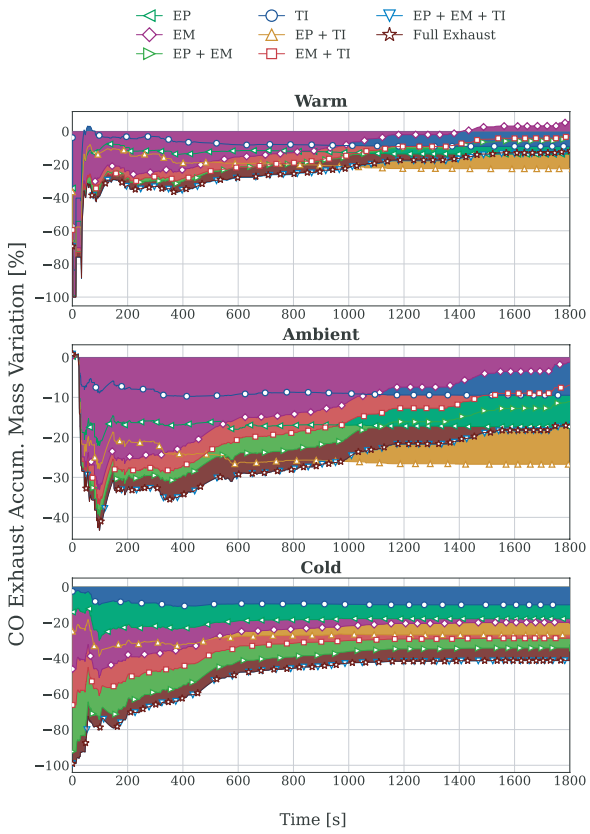

Figure 13. WLTC CO accumulated emissions variation downstream the after-treatment system.

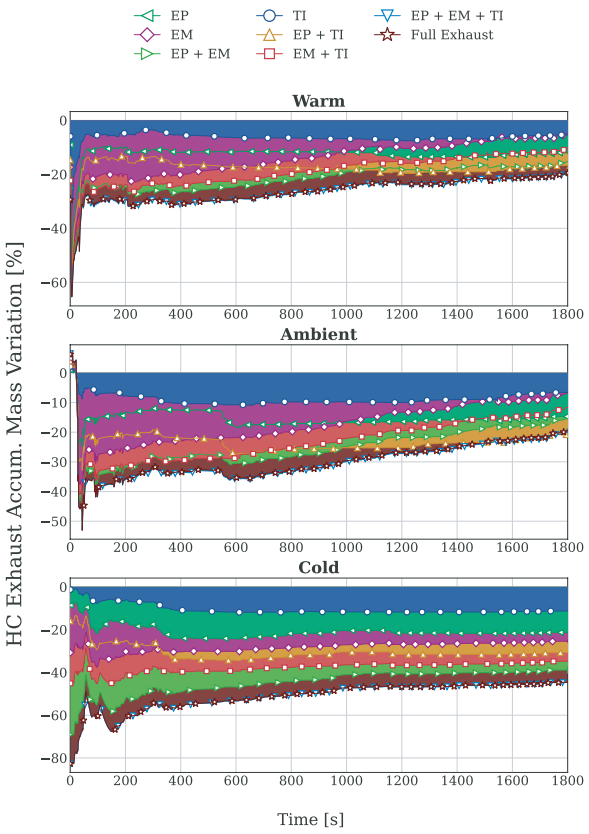

Figure 15. WLTC HC accumulated emissions variation downstream the after-treatment system.

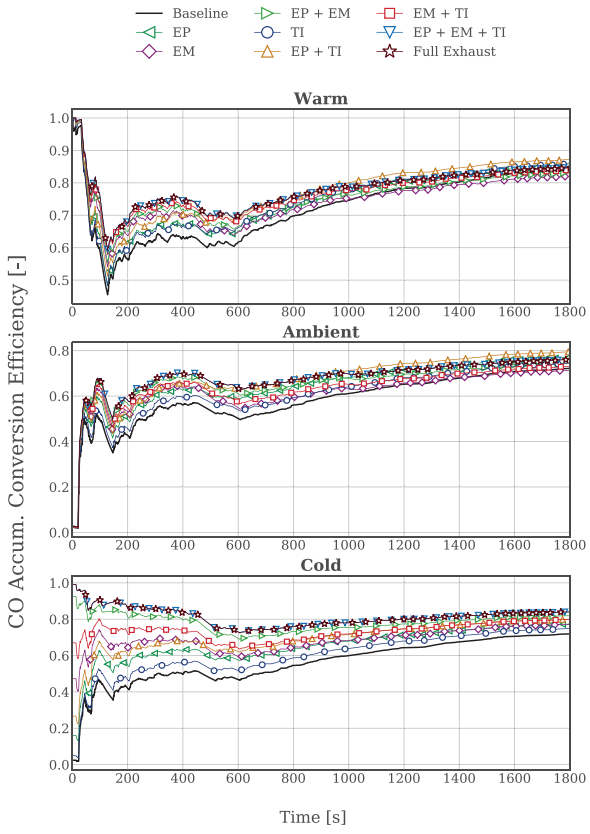

Figure 14. WLTC CO accumulated conversion efficiency.

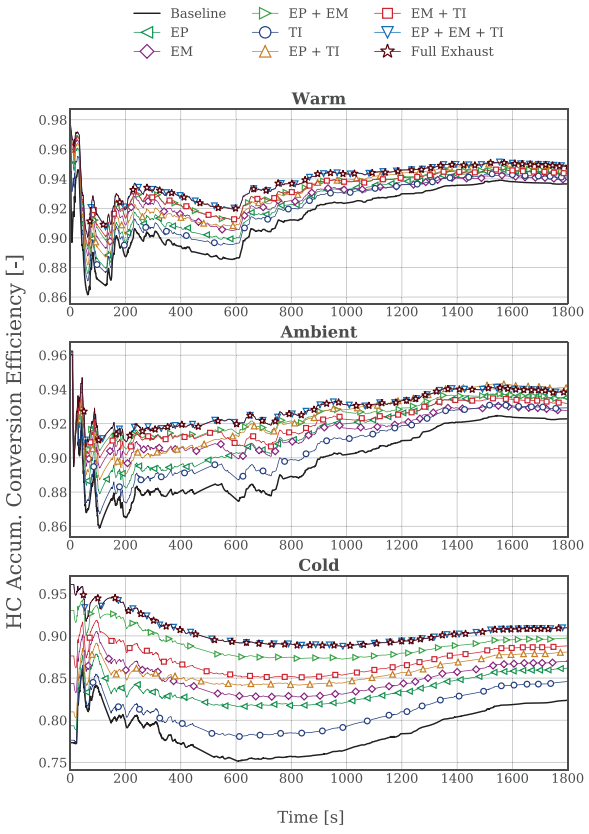

Figure 16. WLTC HC accumulated conversion efficiency.

WLTC. As it was expected, the increment in the exhaust temperature accelerates the light-off in the diesel catalyst, meaning that optimum values for the HC and CO conversion efficiencies are reached faster. This effect is observed in

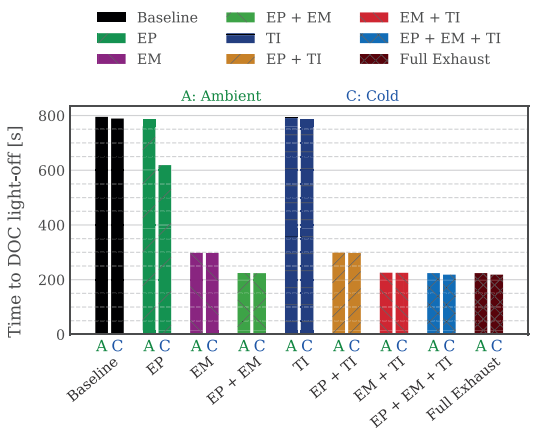

(a) Time to reach the DOC light-off temperature.

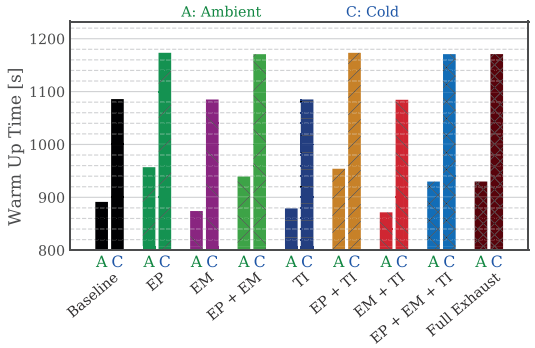

(b) Time to reach coolant thermostat threshold (80 °C)

Figure 17. Time to reach light-off temperature and warm-up time when simulating the WLTC.

Figure 14 where the CO accumulated conversion efficiency is a 12%, 14% and 45% higher at the *Full Exhaust* case at *Warm*, *Ambient* and *Cold* conditions, respectively, at its maximum difference respect to the *Baseline* case. The maximum CO accumulated conversion efficiency increases along the cycle, hence the shape of the CO mass graphs, from the middle of the cycle onwards, the major part of the CO is oxidized.

The same trend is observed for the after-treatment outlet HC emissions in Figure 15. The *Full Exhaust* configuration is presented as the cleanest option due to the increase in the HC conversion efficiency (Figure 16). In this case, a reduction of 44% in HC emissions can be achieved at *Cold* conditions, where the exhaust insulation shows its great potential for two reasons. On one hand, due to the greater pollutants formation at low temperatures; on the other hand, because of the greater time to heat up the DOC at low temperatures.

The lower emissions are targeted by the configurations that achieve a greater increment in the exhaust gases enthalpy. In this case, a complete insulation in the exhaust line outlines the cleanest alternative, presenting a 16% and a 41% reduction of CO at room temperatures of 20°C and −7°C, respectively. In terms of HC emissions, it presents a reduction of 19% at 20°C and 45% at −7°C. As stated above, there is no difference between this case and keeping the turbine housing unaltered (*EP* + *EM* + *TI*).

The emissions results presented in Figures 13 and 15 are the result of an increment in the DOC temperature. The different insulation configurations have a considerable impact in the light-off time as shown in Figure 17a. The results shown a mean time reduction from the 800 seconds of the *Baseline* case to 220-300 seconds for the combined insulation alternatives, which represents a 72 per cent reduction in time for the *EP* + *EM*, *EM* + *TI*, *EP* + *EM* + *TI* and *Full Exhaust* cases. The turbine internal insulation *TI* does not have any impact on the light-off time improvement.

Figure 17b shows the time required for each configuration to reach around 80°C in the coolant temperature at the engine outlet. At this temperature, the coolant starts to be funneled through the radiator branch of the coolant circuit to stabilize its temperature around this value. As inferred from Figure 11, insulating the exhaust ports results in a decrement in the coolant temperature; thus, increasing the warm-up time by 65 seconds at *Ambient* and 87 seconds at *Cold* with the *EP* alternative (an increase of 7.3% and 8.0%, respectively). Only a slight improvement in the engine warm-up time of 20 seconds (-2.3% variation) is achieved by insulating the exhaust manifold and the turbine internal layer at *Ambient* conditions. The rest of alternatives get a small increment of this time, though this increment is about a minute and does not make a substantive difference.

The graphs shown in Figure 18 presents the accumulated CO, HC and fuel consumed as a function of the accumulated gas enthalpy gain. The values are the final cumulative values for each case relative to the *Baseline* case and presented as a percentage. In all three sub-figures a trend can be observed: the greater the enthalpy gain, the lower the CO and HC emissions and the lower the fuel consumed. Regarding fuel consumption, there is not much improvement in fuel economy, specially at *Cold* and *Ambient* conditions. The *TI* alternative show some minor fuel penalty lower than a 1%. This penalty is due to the increase in pumping losses, as reflected in Figure 19, where the internal turbine insulation shows up to a 13% in pumping losses at low speed and load (Figure 19a) and almost 4% at high speed and load (Figure 19b). Insulating the internal surface of the turbine volute makes the VGT close, thus increasing the turbine inlet pressure and increasing the pumping losses. In the same way, pumping losses are higher in the *EM* + *TI* and *EP* + *TI* cases than in the *EM* and *EP* cases. In fact, the fuel variations in Figure 18a are the result of the pumping losses variation in Figure 19. In the cases where the pumping losses are lower than the *Baseline*, there is a small decrease in fuel consumption.

In spite of the little contribution of *TI* in the exhaust gas enthalpy, in combination with the insulation of the exhaust manifold or the exhaust ports, it allows obtaining intermediate results between both *EM* and *EP*, and *Full Exhaust* configurations. As it can be observed in Figure 18a, is it slightly profitable the *EP* + *TI* configuration rather than *EM* + *TI*. *EP* + *TI* obtains a higher increase in the exhaust gas enthalpy, specially when the room temperature is −7°C. When combining both solutions in case *EP* + *TI* the VGT is more opened, so the pumping losses result even more reduced, as shown in Figure 19b and the expansion ratio in the turbine is also lower, causing a smaller drop in temperature from inlet to outlet. If only the low speed stage

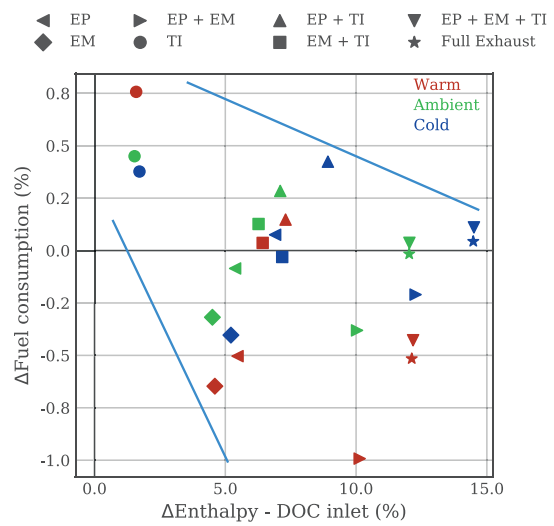

(a) Fuel consumption variation versus exhaust enthalpy variation.

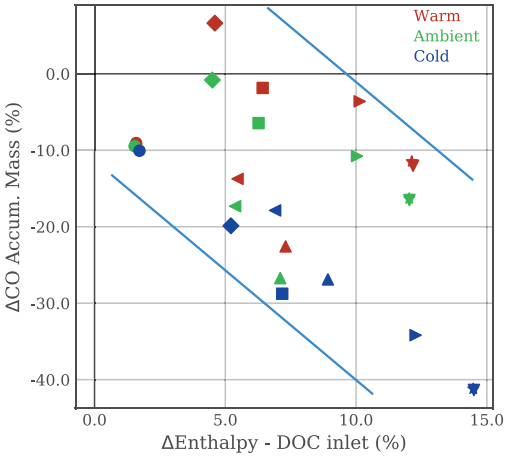

(b) CO emissions variation versus exhaust enthalpy variation.

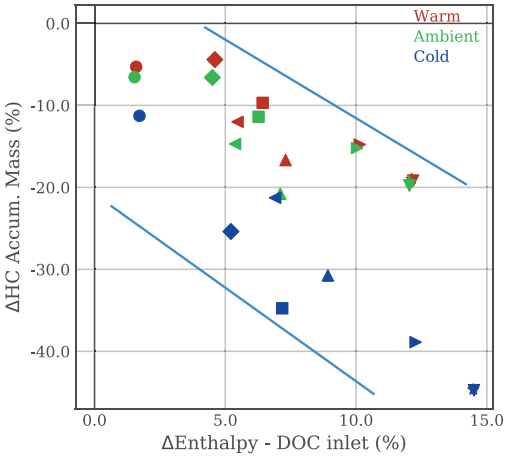

(c) HC emissions variation versus exhaust enthalpy variation.

Figure 18. Accumulated fuel consumption, CO and HC emissions versus accumulated exhaust enthalpy. The variations are calculated taking the baseline case as the reference

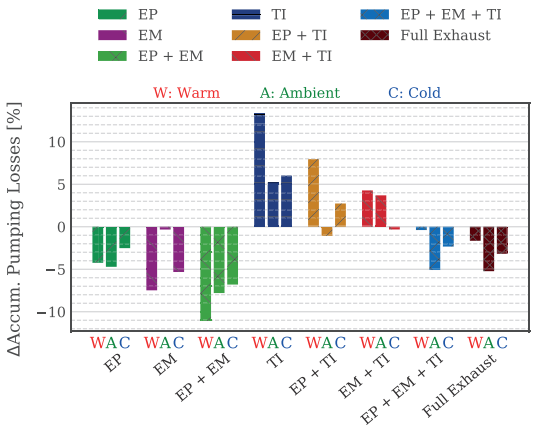

(a) Accumulated pumping losses variation over the low speed stage of the WLTC

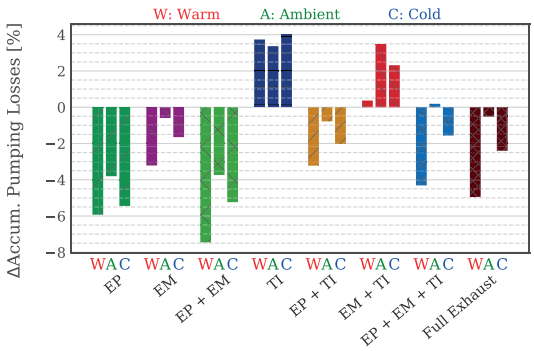

(b) Accumulated pumping losses variation over the extra high speed stage of the WLTC

Figure 19. Accumulated pumping losses variation taking the baseline case as the reference.

of the WLTC is considered, probably, *EM + TI* case would be more profitable, since the enthalpy gain during this stage is greater in Figure 10 and the pumping losses are lower than *EP + TI* case, as can be seen in Figure 19a.

In terms of pollutant emissions reduction, positive results are observable. Great emissions reductions can be obtained at *Cold* conditions by insulating the exhaust manifold as well as the exhaust ports, reducing up to a 40% these emissions. At *Warm* and *Ambient* conditions, since the use of the EGR is more extensive and the DOC is hot for a longer period of time, the total reduction potential is lower, achieving a reduction between 5 and 15% for CO emissions and 5 to 20% for HC emissions.

Summary and conclusions

Several exhaust thermal insulation alternatives have been discussed in this paper with the aim of achieving an increment in the exhaust temperature. In order to have an idea of the maximum exhaust enthalpy gain, the different parts along the exhaust line between the engine and the diesel catalyst have been considered adiabatic. These alternatives have been compared in terms of exhaust temperature profit, fuel consumption, warm-up and light-off time and pollutant emissions at three different temperature conditions. To carry

out this study a one-dimensional engine model has been developed and exploited to simulate the different exhaust insulation configurations at transient (WLTC) conditions of speed and load. For the sake of summarizing the conclusions obtained, the following points are exposed:

1. All the exhaust insulation configurations achieve an increment in the exhaust gas temperature. Hence, the DOC efficiency is increased and lower pollutant emission levels are expelled to the environment.
2. A 20% reduction in CO emissions can be obtained by insulating just the exhaust ports or the exhaust manifold at cold conditions. Regarding HC emissions, this reduction can increase up to 25%. The CO and HC emissions reduction can surpass the 40% by insulating both elements.
3. The insulation of the exhaust manifold leads to a high reduction in the time to reach DOC light-off. The combined insulation of the exhausts ports and the exhaust manifold may reach the light-off time up to 575 second earlier than in the *Baseline* case.
4. On the contrary, insulating the exhaust ports increases the warm-up time since part of the heat cannot be recovered by the coolant circuit. This increase goes up to 65 seconds at *Ambient* conditions and 87 seconds at *Cold* conditions, which represents an increase of 7.3% and 8.0%, respectively.
5. In terms of fuel consumption there is no evident improvement. Only around 1% gain in fuel economy can be achieved the insulating the exhaust ports and the exhaust manifold at warm conditions.
6. The turbine insulation alternatives do not present remarkable benefits, since it is more profitable to insulate the elements close to the engine. However, by also insulating the inner part of the turbine housing, the effectiveness of the exhaust ports insulation is increased. The same happens when combining the exhaust manifold insulation and the turbine internal insulation, specially the low speed stage of the WLTC.

Future works will be focused on improving the prediction of CO and unburned hydrocarbons given by the neural network. This can be achieved by training the network with data in dynamic conditions of speed and load, and at different test bench temperatures.

Regarding the potential of TBC in increasing the exhaust gas temperature, realistic TBC will be considered for the thermal insulation of exhausts ports, exhaust manifold and the turbine internal casing layer. The adiabatic assumption has been considered as an approach to determine which parts of the exhaust line could take advantage of the insulation process.

Funding

This research has been partially funded by the European Union's Horizon 2020 Framework Programme for research, technological development and demonstration under grant agreement 723976 ("DiePeR") and by the Spanish government under the grant agreement TRA2017-89894-R ("Mecoem"). Ángel Auñón was supported through the "Apoyo para la investigación y Desarrollo (PAID)" grant for doctoral studies (FPI S2 2018 1048) by Universitat Politècnica de València.

Declaration of conflicting interests

The author(s) declared no potential conflicts of interest with respect to the research, authorship, and/or publication of this article.

References

1. Hooftman N, Messagie M, Mierlo] JV et al. A review of the european passenger car regulations – real driving emissions vs local air quality. *Renewable and Sustainable Energy Reviews* 2018; 86: 1 – 21. DOI:10.1016/j.rser.2018.01.012.
2. Arnau FJ, Martín J, Pla B et al. Diesel engine optimization and exhaust thermal management by means of variable valve train strategies. *International Journal of Engine Research* 2020; DOI:10.1177/1468087419894804.
3. Luján JM, Serrano JR, Piqueras P et al. Experimental assessment of a pre-turbo aftertreatment configuration in a single stage turbocharged diesel engine. part 2: Transient operation. *Energy* 2015; 80: 614 – 627. DOI:10.1016/j.energy.2014.12.017.
4. Kamo R and Bryzik W. Adiabatic Turbocompound Engine Performance Prediction. SAE Technical Paper 780068, SAE International. DOI:10.4271/780068.
5. Sekar R, Kamo R and Wood J. Advanced Adiabatic Diesel Engine for Passenger Cars. SAE Technical Paper 840434, SAE International. DOI:10.4271/840434.
6. Olmeda P, Martín J, Novella R et al. Assessing the optimum combustion under constrained conditions. *International Journal of Engine Research* 2020; 21(5): 811–823. DOI:10.1177/1468087418814086.
7. Kawaguchi A, Wakisaka Y, Nishikawa N et al. Thermo-swing insulation to reduce heat loss from the combustion chamber wall of a diesel engine. *International Journal of Engine Research* 2019; 20(7): 805–816. DOI:10.1177/1468087419852013.
8. Gingrich E, Tess M, Korivi V et al. The impact of piston thermal barrier coating roughness on high-load diesel operation. *International Journal of Engine Research* 2019; DOI:10.1177/1468087419893487.
9. Powell T, O'Donnell R, Hoffman M et al. Experimental investigation of the relationship between thermal barrier coating structured porosity and homogeneous charge compression ignition engine combustion. *International Journal of Engine Research* 2019; DOI:10.1177/1468087419843752.
10. Somhorst J, Oevermann M, Bovo M et al. Evaluation of thermal barrier coatings and surface roughness in a single-cylinder light-duty diesel engine. *International Journal of Engine Research* 2019; DOI:10.1177/1468087419875837.
11. Poubeau A, Vauvy A, Duffour F et al. Modeling investigation of thermal insulation approaches for low heat rejection diesel engines using a conjugate heat transfer model. *International Journal of Engine Research* 2019; 20(1): 92–104. DOI:10.1177/1468087418818264.
12. Ekström M, Thibblin A, Tjernberg A et al. Evaluation of internal thermal barrier coatings for exhaust manifolds. *Surface and Coatings Technology* 2015; 272: 198 – 212. DOI:10.1016/j.surfcoat.2015.04.005.
13. Thibblin A and Olofsson U. A test rig for evaluating thermal cyclic life and effectiveness of thermal barrier coatings inside exhaust manifolds. In *WCX SAE World Congress Experience*. SAE International. DOI:10.4271/2019-01-0929.

14. Kishi N, Hashimoto H, Fujimori K et al. Development of the Ultra Low Heat Capacity and Highly Insulating (ULOC) Exhaust Manifold for ULEV. In *International Congress and Exposition*. SAE International. DOI:0.4271/980937.
15. Zidat S and Parmentier M. Exhaust Manifold Design to Minimize Catalyst Light-off Time. In *SAE 2003 World Congress and Exhibition*. SAE International. DOI:10.4271/2003-01-0940.
16. Serrano JR, Arnau FJ, Martin J et al. Analysis of Engine Walls Thermal Insulation: Performance and Emissions. In *SAE 2015 World Congress & Exhibition*. SAE International. DOI:10.4271/2015-01-1660.
17. Luján JM, Serrano JR, Piqueras P et al. Turbine and exhaust ports thermal insulation impact on the engine efficiency and aftertreatment inlet temperature. *Applied Energy* 2019; 240: 409 – 423. DOI:10.1016/j.apenergy.2019.02.043.
18. Payri F, Arnau F, Piqueras P et al. Lumped Approach for Flow-Through and Wall-Flow Monolithic Reactors Modelling for Real-Time Automotive Applications. In *WCX World Congress Experience*. SAE International. DOI:10.4271/2018-01-0954.
19. Martín J, Arnau F, Piqueras P et al. Development of an Integrated Virtual Engine Model to Simulate New Standard Testing Cycles. In *WCX World Congress Experience*. SAE International. DOI:10.4271/2018-01-1413.
20. Serrano JR, Arnau F, García-Cuevas L et al. Development and validation of a radial turbine efficiency and mass flow model at design and off-design conditions. *Energy Conversion and Management* 2016; 128: 281–293. DOI:10.1016/j.enconman.2016.09.032.
21. Galindo J, Tiseira A, Navarro R et al. Compressor Efficiency Extrapolation for 0D-1D Engine Simulations. In *SAE 2016 World Congress and Exhibition*. SAE International. DOI:10.4271/2016-01-0554.
22. Serrano JR, Olmeda P, Arnau F et al. A holistic methodology to correct heat transfer and bearing friction losses from hot turbocharger maps in order to obtain adiabatic efficiency of the turbomachinery. *International Journal of Engine Research* 2019; DOI:10.1177/1468087419834194.
23. Serrano JR, Olmeda P, Arnau FJ et al. Analysis and Methodology to Characterize Heat Transfer Phenomena in Automotive Turbochargers. *Journal of Engineering for Gas Turbines and Power* 2014; 137(2). DOI:10.1115/1.4028261.
24. Serrano JR, Olmeda P, Arnau FJ et al. Turbocharger heat transfer and mechanical losses influence in predicting engines performance by using one-dimensional simulation codes. *Energy* 2015; 86: 204 – 218. DOI:10.1016/j.energy.2015.03.130.
25. Arrègle J, López JJ, Martín J et al. Development of a Mixing and Combustion Zero-Dimensional Model for Diesel Engines. In *SAE 2006 World Congress and Exhibition*. SAE International. DOI:10.4271/2006-01-1382.
26. Payri F, Arrègle J, López JJ et al. Diesel NOx Modeling with a Reduction Mechanism for the Initial NOx Coming from EGR or Re-entrained Burned Gases. In *SAE World Congress and Exhibition*. SAE International. DOI:10.4271/2008-01-1188.
27. Broatch A, Olmeda P, Martín J et al. Development and Validation of a Submodel for Thermal Exchanges in the Hydraulic Circuits of a Global Engine Model. In *WCX World Congress Experience*. SAE International. DOI:10.4271/2018-01-0160.
28. Deppenkemper K, Özyalcin C, Ehrly M et al. 1D Engine Simulation Approach for Optimizing Engine and Exhaust Aftertreatment Thermal Management for Passenger Car Diesel Engines by Means of Variable Valve Train (VVT) Applications. In *WCX World Congress Experience*. SAE International. DOI:10.4271/2018-01-0163.
29. Guardiola C, Pla B, Bares P et al. An on-board method to estimate the light-off temperature of diesel oxidation catalysts. *International Journal of Engine Research* 2018; DOI:10.1177/1468087418817965.
30. Russell A and Epling W. Diesel Oxidation Catalysts. *Catalysis Reviews* 2011; 53(4): 337–423. DOI:10.1080/01614940.2011.596429.
31. Guardiola C, Pla B, Piqueras P et al. Model-based passive and active diagnostics strategies for diesel oxidation catalysts. *Applied Thermal Engineering* 2017; 110: 962 – 971. DOI:10.1016/j.applthermaleng.2016.08.207.
32. Abdelghaffar WA, Osman MM, Saeed MN et al. Effects of Coolant Temperature on the Performance and Emissions of a Diesel Engine. In *ASME 2002 Internal Combustion Engine Division Spring Technical Conference*. ICES2002-464, pp. 187–197. DOI:10.1115/ICES2002-464.
33. Torregrosa A, Olmeda P, Martín J et al. Experiments on the influence of inlet charge and coolant temperature on performance and emissions of a DI Diesel engine. *Experimental Thermal and Fluid Science* 2006; 30(7): 633 – 641. DOI:10.1016/j.expthermflusci.2006.01.002.

Nomenclature

List of abbreviations

0D	Zero-dimensional
1D	One-dimensional
BSFC	Brake Specific Fuel Consumption
CO	Carbon monoxide
DOC	Diesel Oxidation Catalyst
DPF	Diesel Particle Filter
EAT	Exhaust After-Treatment
ECU	Engine Control Unit
EGR	Exhaust Gas Recirculation
HC	Hydrocarbons
HP-EGR	High Pressure EGR
HSDI	High Speed Direct Injection
IMEP	Indicated Mean Effective Pressure
LP-EGR	Low Pressure EGR
NO_x	Nitrogen oxides
TBC	Thermal Barrier Coating
VEMOD	Virtual Engine Model
VGT	Variable Geometry Turbine
WLTC	Worldwide Harmonized Light-Duty Vehicles Test Cycle